**Proceedings of the ASME 2023 18th International
Manufacturing Science and Engineering Conference
MSEC 2023
June 12-16, 2023, New Brunswick, New Jersey, USA**

MSEC2023-103321

THE EFFECT OF VOLTAGE ON THE INITIATION OF NATURAL PULSATION IN ELECTROHYDRODYNAMIC JET PRINTING - DRAFT

Angelo Hawa [1], **Ali Bahrami** [1], **Kira Barton** [1,2]
[1] Department of Mechanical Engineering
[2] Department of Robotics
University of Michigan
Ann Arbor, Michigan 48109

ABSTRACT

Electrohydrodynamic jet (e-jet) printing is a high-resolution additive manufacturing process that uses an electric field to extract polarizable ink from a nozzle. The high-resolution capabilities of e-jet printing are very favorable for the fabrication of printed electronics and biosensors, which is typically achieved using a highly controllable pulsating jet. In this regime, high voltage pulses are superimposed over a baseline DC voltage, which primes the meniscus for the subsequent pulse. While a higher baseline voltage reduces the response time of the system, values above a certain threshold can cause the printing to transition toward an uncontrollable jetting regime in which the natural dynamics of the ink instigate pulsating jet behavior. To characterize the effect of these unwanted transitions on the final print, key parameters of the natural pulsating jet mode must be identified. This work presents findings on the relevant time constants and volume measurements of jet printing at various subcritical voltages. While the impingement time of the jet was found to be proportional to the applied voltage, the volume of the initial droplet increasingly varied. Conclusions regarding permissible pulse widths and system predictability as a function of voltage were made.

1 Introduction

Additive manufacturing (AM) is the layer-by-layer process of merging materials together using an energy source [1]. Compared to traditional manufacturing techniques, AM has the capability to fabricate more complex devices with a far greater efficiency and less material waste [2]. Recent advancements in AM have improved the precision of micro- and nano-scale devices, which constitute numerous applications across a variety of engineering disciplines. Electrohydrodynamic jet (e-jet) printing is an emerging AM technique that demonstrates promising properties for micro-scale fabrication. With resolution capabilities reaching below 100 nm [3, 4], e-jet has been favored as the printing method for various applications, such as printed electronics [5, 6], biosensors [7, 8], and tissue engineering [9, 10].

During the e-jet printing process, a potential difference is applied between the conductive micro-nozzle and the grounded substrate. As a result, mobile charges within the ink begin to accumulate on the ink-air interface until the meniscus deforms into a Taylor cone. As the potential difference further increases, the Coulombic repulsion between the mobile ions overcomes the surface tension of the ink, and a discrete jet is released. In contrast with traditional inkjet printing techniques, the deposited droplet size can be several orders of magnitude smaller than the nozzle [11]. Figure 1(a) presents a labelled schematic diagram of a sample e-jet printer used for experimental analysis.

Various regimes of e-jet printing have been identified using a set of dimensionless parameters as a function of applied voltage and nozzle flow rate [12]. The vast majority of device fabrication utilizes the cone-jet regime, characterized by the steady emission of a contiguous jet of ink from the nozzle. Drop-on-demand printing can be achieved through custom modification of the input shape of the applied voltage, which typically involves

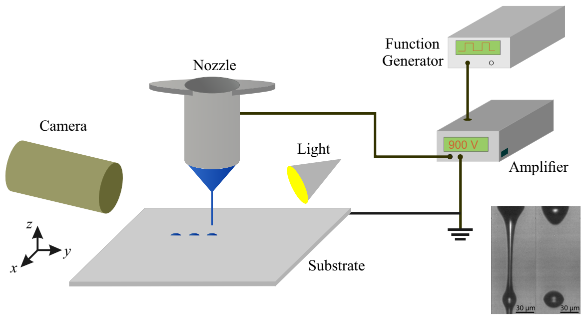

(a)

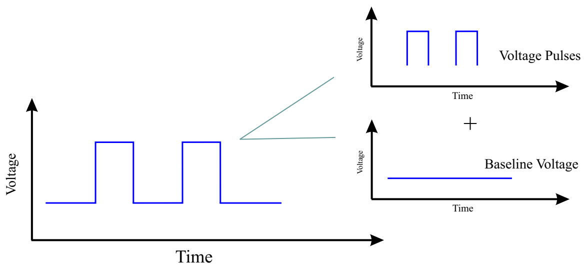

(b)

FIGURE 1: (a) Schematic figure of an e-jet printing setup and (b) an illustration of the signal pulse decomposition.

the alternation of two or more voltages at varying pulse widths. As a mechanism for reducing the response time of the system, baseline voltages which do not instigate droplet ejection are used in conjunction with high voltage pulses. A illustrated decomposition of the voltage signals used in pulse printing is provided in Fig. 1(b).

Although the high-resolution properties of e-jet printing are favorable for a wide variety of micro-scale applications, one factor that hinders its commercial expansion is a relatively low production speed [13]. Therefore, efforts to foster a greater manufacturing speed are indispensable. Choi and Khan demonstrated that a multi-nozzle printer setup can be used to accomplish this [14, 15]; however, the velocity of the ejected droplet is dictated by various material properties of the ink and the system inputs. Though the system inputs can be adjusted [16], there is also an upper limit for their impact on the printing behavior. The applied high voltage is constrained by the potential to transition toward less controllable printing regimes, such as multi-jet or tilted jet [11]. Additionally, Stachewicz et.al. [17] demonstrated that the pulse frequency is confined by the hydrodynamic behavior inside the capillary. One potential solution which has not been widely studied is the effect of the baseline voltage, which is commonly used to prime the meniscus for the subsequent pulse, lowering the response time of the system. However, the upper limit of this input is limited by the transition toward an uncontrollable regime known as natural pulsation.

The natural pulsation regime occurs when the applied voltage exceeds the threshold for droplet ejection, but falls below the critical value required for a sustained cone-jet. This regime is characterized by an initial deposit followed by the natural repetitive process of jet breakup, retraction, charge accumulation, and jet impingement [18]. Empirical analysis on the steady state behavior of this regime has been widely performed, and the relationships between jet diameter and pulsation frequency as a function of applied voltage are well established [19]. However, these studies disregard the characteristics of the initial deposition, which differ from steady state behavior. Defining certain aspects of this regime's initialization allows for the use of natural pulsation voltages as the baseline voltage in pulse printing, which reduces the response time of the system. Specifically, the elapsed time between the voltage pulse and jet impingement provides insight into the appropriate design parameters of the voltage input shape. Additionally, the consistency of the initial deposit's volume following natural breakup indicates the controllability of the system in this state.

This paper presents a case study on the relevant time constants and volume measurements of the natural pulsation regime with regards to manufacturing applications. The main contributions of this work are (1) Identifying the maximum length of time a natural pulsation voltage can be applied until droplet ejection occurs and (2) Characterizing the predictability of the initial droplet size in the natural pulsation regime. The rest of the paper is organized as follows: Section 2 provides descriptions of the experimental setup and methods, Section 3 outlines the experimental results, and Section 4 contains concluding arguments and details future work.

2 Materials and Methods

2.1 Experimental Setup

All experiments are performed using a custom-built e-jet printer developed by the Barton Research Group. The setup consists of a motion system, a print head, and high-speed imaging equipment. For the motion system, a single-axis lift stage (Aerotech, ANT130) is superimposed on a two axis linear stage (Aerotech, $Planar_{DL}$) to provide controlled X-Y-Z positioning of the silicon wafer substrate. The wafer rests suctioned on an electrically-grounded aluminum disc. A custom 3D printed syringe holder containing high voltage electrical connections is mounted on the print head, where a servomotor controls its Z-axis location (Aerotech, BMS60). Mounted adjacent to the motion system is a high-speed camera (Vision Research, Phantom VEO-410L) and a high intensity coaxial LED light (Advanced Illumination, SL162).

The substrate is a silicon wafer with a resistivity of 0.005-0.02 Ohm-cm. Three glass nozzles with inner diameters of 30 μm are sputter coated with 0.05 nm gold to ensure good conductivity. The printing ink is Norland Optical Adhesive (NOA) 81,

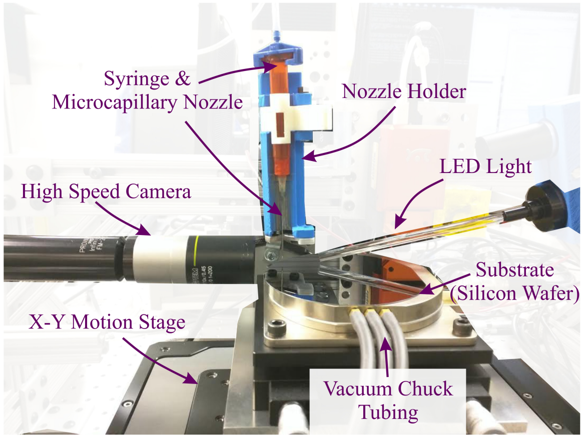

FIGURE 2: The experimental setup used for printing.

a dielectric polymer.

The nozzle's electric potential is generated using a voltage amplifier (TREK, 677B) and controlled with a function generator (RIGOL, DG1032Z), which supplies the triggering mechanism for the high-speed imaging. The voltage waveform is monitored using an oscilloscope (Tektronix, TDS 2024B).

The nozzle is positioned 150 μm above the substrate. The high-speed camera is configured to record at 10,000 Hz to fully capture the jetting dynamics. Due to the chosen frame rate, the sample time is constrained to 741 ms. Because typical pulse printing occurs at time scales of less than 10^2 ms [20], this constraint does not impact the analysis of the experimental results, and a high voltage pulse of 741 ms is applied to initiate natural pulsation. Each frame has a 1024 by 512 pixel size and is captured with an exposure time of 99 μs. A 100x lens attachment provides a resolution of 0.2 $\frac{\mu m}{px}$. A labeled image of the experimental setup is provided in Fig. 2.

2.2 Experimental Procedure

As part of the initialization process for each nozzle, DC voltages ranging from 1000V to 1200V are applied for several minutes while the substrate is moved in a raster formation. A continuous jet is maintained throughout the duration of this process, which serves as a method for clearing potential blockages within the nozzle. To record a lower bound for the experimental voltages, the applied voltage is gradually increased from zero until initial jet formation. Due to the similarity of initiation voltages, an experimental lower bound of 700 V is chosen for each nozzle. Three trials at increasing increments of 50 V starting from 700 V are recorded until continuous jet behavior was observed. The triggering signal for the high-speed camera is coupled with the applied voltage pulse.

2.3 High-Speed Video Image Processing

In order to extract volume measurements of the initial deposited droplets, image processing techniques with MATLAB are used to outline the droplet contour in each frame. Minimal user-defined regions are required to assist the algorithms. The computation steps along with their corresponding MATLAB functions are provided below.

1) **Convert 3D Grayscale Image to Binary:** A locally adaptive threshold (`adaptthresh`) with a tolerance of 0.55 is computed for each frame and used in correspondence with MATLAB's binary conversion function (`imbinarize`). This step results in the foreground objects (ink and nozzle) appearing black in front of a white background.

2) **Apply a Noise Filter:** The droplet boundary tracing algorithm dictates that the image pixels in the region below the substrate must contain a value of 0. To achieve this requirement, the user defines a point (`drawpoint`) on an image just below the line corresponding to the substrate. This is found by displaying a frame (`imshow`) where one or more droplets have been deposited and identifying a point just below the line of reflection. Once the frames are cropped, a 2-D median filter (`medfilt2`) is applied to reduce the overall noise of each frame.

3) **Identify Jet-Substrate Contact:** The natural pulsation regime is characterized by cyclic phases of a contiguous ink connection between the nozzle and the substrate followed by the advancement or recession of the jet. When the jet is contacting the substrate, the deposited volume is transient, and volume measurements during this phase require advanced operational procedures. However, the period when the jet is moving above the substrate (whether receding or advancing) defines a constant droplet volume which can be measured. Differentiation of these two phases can be achieved by tracing the interface of the black and white regions of the frames (`bwtraceboundary`) and recording the number of pixels along the boundary. The starting pixel of the boundary tracing is chosen to be the top left corner of the image. Upon application of high voltage, the meniscus retracts toward the substrate, forming a jet, and the length of the boundary increases. The initial frame depicting jet contact with the substrate corresponds to a sharp decline in the boundary length, as the tracing cannot map pixels on the right side of the frame. The instigation of jet breakup then drastically increases the number of traced boundary points. The detection of these abrupt changes (`ischange`) can identify phases of the natural pulsation behavior, and, therefore, define frames when the droplet volume is constant. Sample frames and the progression of the boundary point count are shown in Fig. 3. Note that the sharp changes in the plot provided in Fig. 3(c) correspond to the transition to and from a contiguous jet connecting the nozzle to the substrate. The duration between jet breakup and impingement is known as the contact time of the jet, which directly correlates to the volume of the deposition.

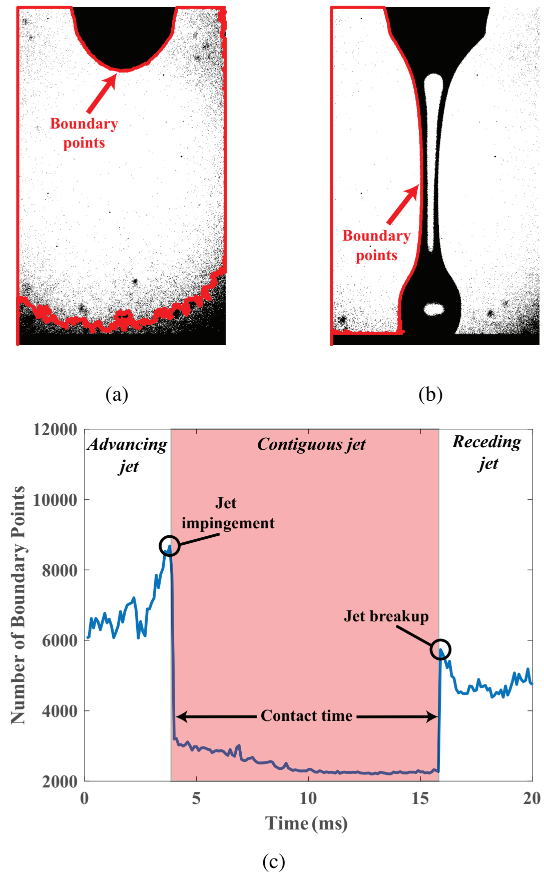

FIGURE 3: Sample frames with traced boundary before (a) and during (b) jet contact with the substrate. (c) Boundary point count progression with labeled regions.

4) **Droplet Contour Modelling and Volume Measurements:** The user defines a rectangle in which the droplet may be found (`drawrectangle`). Boundary points lying within the rectangle constitute the droplet's contour. The droplet's horizontal cross section is assumed to be circular, and the overall shape is modelled as a stack of conical frusta with a height of 1 pixel. The volume of each frustum can be summed, as shown in Eq. 1,

$$V_d = \sum_{i=1}^{n-1} \frac{\pi}{3} (R_i^2 + R_i R_{i+1} + R_{i+1}^2) \quad (1)$$

where V_d is the volume of the deposited droplet [μm^3] and R_i and R_{i+1} are the radii of sequential frusta [μm].

Figure 4 presents a side-by-side comparison of a frame pre- and post-processing. Note that the shaded region in Fig. 4(b) indicates the region modelled by the computer vision algorithm to compute the droplet's volume.

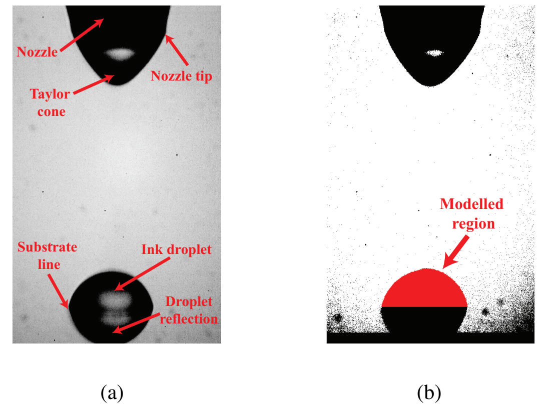

FIGURE 4: (a) Labeled comparison of raw image frame and (b) processed frame used for computer vision algorithm.

3 Results

Figure 5(a) presents a box plot of the initial jet impingement times as a function of the applied voltage. As expected, an inversely proportional relationship exists between these variables. Applying a higher voltage to the nozzle results in a greater charge accumulation rate on the meniscus, and, subsequently, a faster ejection. Additionally, the spread of the impingement times reduces with voltage. This relationship is likely resultant of the unstable jet formation behavior that exists near the critical voltage values required for ejection [21]. The distributions in Fig. 5(a) provide insight into the possible shapes of the applied voltage input. Specifically, a baseline voltage applied for a duration that exceeds the impingement time would result in an undesired ejection. The results imply that a larger range of permissible widths exists for baselines of lower voltage magnitudes. For example, as observed in Fig. 5(a), reducing the baseline voltage from 750 V to 700 V results in a two fold increase in the impingement time, which expands the design space of the input shape. This principle is illustrated in Fig. 6, which depicts a series of high voltage pulses superimposed on baseline voltages of varying magnitudes. Note that the temporal widths of the elevated baseline voltages (τ_2 and τ_3) differ in accordance with their respective voltage magnitudes (V_2 and V_3). To avoid undesired droplet ejection while simultaneously reducing the system response time, these widths must be limited to experimentally-determined impingement times.

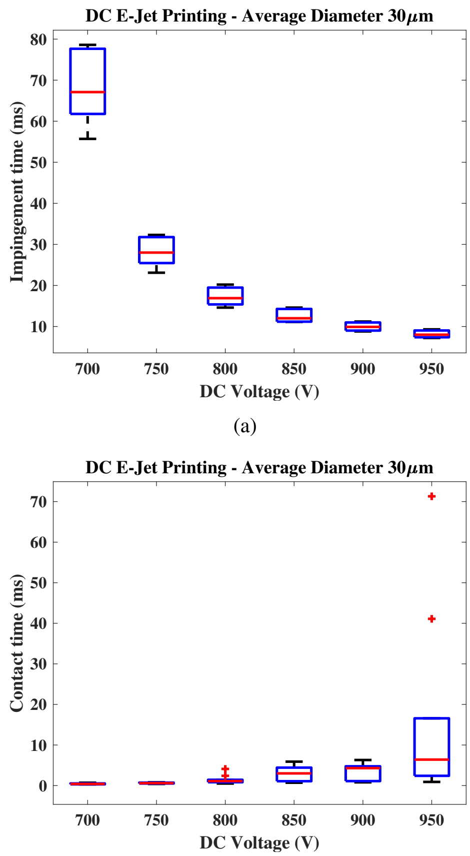

(a)

(b)

FIGURE 5: (a) Summary of the jet impingement times and (b) contact times as a function of applied voltage.

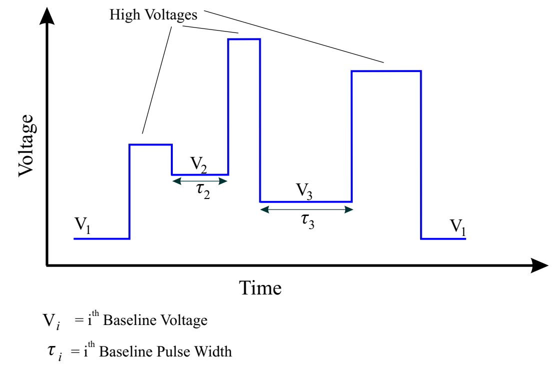

FIGURE 6: A sample applied voltage input shape containing a series of baseline and pulsed voltages.

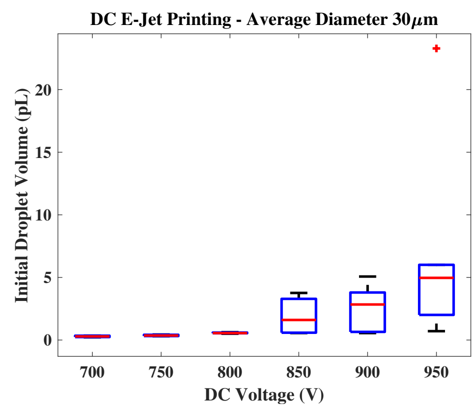

FIGURE 7: Summary of volume measurements of the initial deposition as a function of applied voltage.

Due to the existence of temporal uncertainties for all experimental applied voltages, it becomes pertinent to examine the consequences of surpassing this time constant. The jet's contact time provides insight to the volume of the initial deposition. This parameter is presented as a function of applied voltage in the form of a box plot in Fig. 5(b). In contrast to the inverse relationship seen in Fig. 5(a), the mean value and variance of the contact time are observed to increase with voltage. This result concurs with prior expectations, as the applied voltages near the maximum of the experimental range likely fall within a transition region bordering the natural pulsation and cone-jet regimes.

A box plot displaying these volume measurements is provided in Fig. 7. As expected, these results mimic the functionally increasing behavior of the contact times seen in Fig. 5(b) and indicate proportionality between the applied voltage and the uncertainty of the initial droplet's volume.

It is evident that a trade-off relationship exists regarding the controllability of e-jet printing in the initial moments of the natural pulsation regime. Reducing the applied baseline voltage allows for a greater range of permissible widths and low volumetric uncertainties, but the temporal characteristics associated with jet formation and impingement remain difficult to predict. In contrast, a higher baseline voltage provides a faster system response time, but the volumetric analysis of the initial droplet demonstrates the existence of high uncertainties. Therefore, user-defined preferences for controlled printing must be formulated prior to selecting the natural pulsation baseline voltage.

4 Conclusion and Future Work

While e-jet printing possesses many advantages for microscale fabrication, one limiting factor for wide-scale expansion is the printing speed. A potential mediation for this hindrance is the implementation of the natural pulsation regime in pulse printing. This paper presents a temporal and volumetric analysis of initial jet behavior within the natural pulsation regime. Key trade-off relationships regarding design space freedom, volumetric uncertainty, and jet impingement timing were identified and discussed. Future work will develop quantitative relationships to describe these relationships using dimensionless parameters, automate the computer vision algorithms to require less user input, and use numerical tools such as computational fluid dynamics to model the described behavior.

REFERENCES

[1] Abdulhameed, O., Al-Ahmari, A., Ameen, W., and Mian, S. H., 2019. "Additive manufacturing: Challenges, trends, and applications". *Advances in Mechanical Engineering,* ***11***(2), Feb., p. 168781401882288.

[2] Tofail, S. A. M., Koumoulos, E. P., Bandyopadhyay, A., Bose, S., O'Donoghue, L., and Charitidis, C., 2018. "Additive manufacturing: scientific and technological challenges, market uptake and opportunities". *Materials Today,* ***21***(1), Jan., pp. 22–37.

[3] Park, J.-U., Hardy, M., Kang, S. J., Barton, K., Adair, K., Lee, C. Y., Strano, M. S., Alleyne, A. G., Georgiadis, J. G., Ferreira, P. M., et al., 2007. "High-resolution electrohydrodynamic jet printing". *Nature materials,* ***6***(10), pp. 782–789.

[4] An, S., Stambaugh, C., Kim, G., Lee, M., Kim, Y., Lee, K., and Jhe, W., 2012. "Low-volume liquid delivery and nanolithography using a nanopipette combined with a quartz tuning fork-atomic force microscope". *Nanoscale,* ***4***(20), Sept., pp. 6493–6500.

[5] Choi, K. H., Rahman, K., Muhammad, N. M., Khan, A., Kwon, K.-R., Doh, Y. H., and Kim, H.-C., 2011. "Electrohydrodynamic inkjet – micro pattern fabrication for printed electronics applications".

[6] Jeong, S., Lee, J.-Y., Lee, S. S., Seo, Y.-H., Kim, S.-Y., Park, J.-U., Ryu, B.-H., Yang, W., Moon, J., and Choi, Y., 2013. "Metal salt-derived In–Ga–Zn–O semiconductors incorporating formamide as a novel co-solvent for producing solution-processed, electrohydrodynamic-jet printed, high performance oxide transistors". *Journal of Materials Chemistry C,* ***1***(27), June, pp. 4236–4243.

[7] Pannier, C., Wang, Z., Hoelzle, D., and Barton, K., 2016. "Electrohydrodynamic jet printing: A 3d printing technique for sensor fabrication". pp. 149–152.

[8] Shirsavar, M. A., Taghavimehr, M., Ouedraogo, L. J., Javaheripi, M., Hashemi, N. N., Koushanfar, F., and Montazami, R., 2021. Machine Learning-Assisted E-jet Printing of Organic Flexible Biosensors, Nov. arXiv:2111.03985 [cs].

[9] Wu, Y., Wang, Z., Ying Hsi Fuh, J., San Wong, Y., Wang, W., and San Thian, E., 2017. "Direct E-jet printing of three-dimensional fibrous scaffold for tendon tissue engineering". *Journal of Biomedical Materials Research. Part B, Applied Biomaterials,* ***105***(3), Apr., pp. 616–627.

[10] Liu, T., Huang, R., Zhong, J., Yang, Y., Tan, Z., and Tan, W., 2017. "Control of cell proliferation in E-jet 3D-printed scaffolds for tissue engineering applications: the influence of the cell alignment angle". *Journal of Materials Chemistry B,* ***5***(20), May, pp. 3728–3738.

[11] Onses, M. S., Sutanto, E., Ferreira, P. M., Alleyne, A. G., and Rogers, J. A., 2015. "Mechanisms, capabilities, and applications of high-resolution electrohydrodynamic jet printing". *Small,* ***11***(34), pp. 4237–4266.

[12] Lee, A., Jin, H., Dang, H.-W., Choi, K.-H., and Ahn, K. H., 2013. "Optimization of Experimental Parameters To Determine the Jetting Regimes in Electrohydrodynamic Printing". *Langmuir,* ***29***(44), Nov., pp. 13630–13639.

[13] Khan, A., Rahman, K., Kim, D. S., and Choi, K. H., 2012. "Direct printing of copper conductive micro-tracks by multi-nozzle electrohydrodynamic inkjet printing process". *Journal of Materials Processing Technology,* ***212***(3), pp. 700–706. Micro-Manufacturing Processes.

[14] Choi, K.-H., Khan, A., Rahman, K., Doh, Y.-H., Kim, D.-S., and Kwan, K.-R., 2011. "Effects of nozzles array configuration on cross-talk in multi-nozzle electrohydrodynamic inkjet printing head". *Journal of Electrostatics,* ***69***(4), pp. 380–387.

[15] Khan, A., Rahman, K., Ali, S., Khan, S., Wang, B., and Bermak, A., 2021. "Fabrication of circuits by multi-nozzle electrohydrodynamic inkjet printing for soft wearable electronics". *Journal of Materials Research,* ***36***(18), pp. 3568–3578.

[16] Barton, K., Mishra, S., Alleyne, A., Ferreira, P., and Rogers, J., 2011. "Control of high-resolution electrohydrodynamic jet printing". *Control Engineering Practice,* ***19***(11), pp. 1266–1273.

[17] Stachewicz, U., Yurteri, C. U., Marijnissen, J. C., and Dijksman, J. F., 2009. "Stability regime of pulse frequency for single event electrospraying". *Applied Physics Letters,* ***95***(22), p. 224105.

[18] Spiegel, I. A., Sammons, P., and Barton, K., 2020. "Hybrid Modeling of Electrohydrodynamic Jet Printing". *IEEE Transactions on Control Systems Technology,* ***28***(6), Nov., pp. 2322–2335.

[19] Chen, C.-H., Saville, D. A., and Aksay, I. A., 2006. "Scaling laws for pulsed electrohydrodynamic drop formation". *Applied Physics Letters,* ***89***(12), Sept., p. 124103.

[20] Mishra, S., Barton, K. L., Alleyne, A. G., Ferreira, P. M., and Rogers, J. A., 2010. "High-speed and drop-on-demand printing with a pulsed electrohydrodynamic jet". *Journal of Micromechanics and Microengineering,* ***20***(9), aug, p. 095026.

[21] Li, K., Zhao, Y., Liu, M., Wang, X., Zhang, F., and Wang, D., 2021. "A multi-scale e-jet 3d printing regulated by structured multi-physics field". *Journal of Micromechanics and Microengineering,* ***32***(2), dec, p. 025005.